american physiological society

JNP JOURNAL OF NEUROPHYSIOLOGY

J Neurophysiol 135: 97–109, 2026.
First published December 1, 2025; doi:10.1152/jn.00336.2025

RESEARCH ARTICLE

Control of Movement

Propagation of beta bursts from the motor cortex to the motor units of multiple upper-limb muscles

Cosima Graef,[1,2,3] Alejandro Pascual Valdunciel,[4,5] Dario Farina,[5] Ravi Vaidyanathan,[2,6] Yen F Tai,[2,7,8] and Shlomi Haar[2,8,9]

[1]*Department of Computing, Imperial College London, London, United Kingdom;* [2]*Care, Research & Technology Centre, UK Dementia Research Institute, London, United Kingdom;* [3]*UKRI Centre for Doctoral Training in AI for Healthcare, Imperial College London, London, United Kingdom;* [4]*BSICoS group, I3A Institute and IIS Aragón, University of Zaragoza, Zaragoza, Spain;* [5]*Department of Bioengineering, Imperial College London, London, United Kingdom;* [6]*Department of Mechanical Engineering, Imperial College London, London, United Kingdom;* [7]*Department of Neurology, Charing Cross Hospital, London, United Kingdom;* [8]*Department of Brain Sciences, Imperial College London, London, United Kingdom; and* [9]*School of Psychology, University of Surrey, Guildford, United Kingdom*

Abstract

Beta band (13–30 Hz) oscillations have been closely associated with motor control, yet their precise functional significance remains a subject of debate. Recent research suggests that beta activity occurs in transient bursts, which may better capture its role in movement regulation than sustained oscillations. Although cortical and subcortical beta bursts have been extensively studied, their transmission to muscles—particularly in the upper limb—remains poorly understood and has been limited by traditional bipolar EMG techniques. In this study, we used high-density surface electromyography (HDsEMG) and electroencephalography (EEG) to investigate the cortico-peripheral dynamics of beta bursts in forearm extensor muscles during isometric contractions at the motor unit (MU) level. We show that MU activity in the upper limb exhibits discrete beta bursts that are temporally aligned with cortical beta activity. Notably, beta bursts in the periphery were time-locked to cortical bursts, suggesting strong coordination and synchronization of bursting across the corticospinal tract. We also found stronger beta synchronization in the extensor's ulnar regions compared with the radial regions, indicating muscle-specific differences in beta projections to the motor neuron pools. These findings provide the first demonstration of beta burst propagation from cortex to upper-limb MUs and show that HDsEMG can reliability detect such events in the upper limb. This work supports the cortical origin and structure of peripheral beta activity and demonstrates its potential as a neurophysiological biomarker for targeting corticospinal dynamics in motor disorders such as Parkinson's disease.

NEW & NOTEWORTHY We provide the first evidence of cortical beta bursting in motor unit (MU) activity of forearm extensors across force levels. MU beta bursts are time-locked to cortical beta bursts, supporting direct corticospinal transmission in the upper limb. Our findings indicate that burst timing is robust to changes in contraction levels and demonstrate a robust cortical-peripheral beta relationship during isometric contractions. They also reinforce the utility of HDsEMG for investigating burst dynamics and refining neurophysiological biomarkers.

beta bursts; corticomuscular coherence; electroencephalography; electromyography; motor units

INTRODUCTION

Oscillatory activity in the beta frequency range (13–30 Hz) plays a fundamental role in motor control. It has traditionally been thought to stabilize and maintain consistent motor output (1), while its synchrony between the motor cortex and muscles supports the fine-tuning of ongoing movements (2). However, recent evidence suggests that beta activity is not sustained continuously but instead occurs in brief, transient bursts (3), a concept anticipated in earlier reports of "waxing

Correspondence: S. Haar (s.haar@imperial.ac.uk).
Submitted 1 July 2025 / Revised 4 August 2025 / Accepted 24 November 2025

and waning" beta oscillations during sustained contractions (4, 5). Although a substantial body of work has described neural beta bursts in M1 and electroencephalography (EEG) (6, 7), comparatively little is known about how such bursting is expressed in the periphery. Beta bursts encode functionally relevant information for movement initiation (8) and performance (9), and are implicated in motor disorders such as Parkinson's disease (PD) (10, 11). Although most research on pathological beta activity has focused on the subthalamic nucleus (STN) (11), cortical beta bursts also play a significant role in motor processing (12–14). Notably, treatments like levodopa and deep brain stimulation (DBS) can reduce beta burst duration and rate, with beta-sensitive closed-loop DBS approaches being explored at both cortical and STN levels (10, 11, 15–18). A recent study found that cortical bursts precede STN bursts and better relate to worsening bradykinesia (19), highlighting the importance of tracking beta burst propagation.

Cortical beta activity propagates to the periphery via corticospinal pathways, and its coupling with contralateral muscle activity during steady isometric contraction is evident in the corticomuscular coherence (CMC), which peaks in the beta frequency range (20, 21). Early work in the 1990s demonstrated significant beta-band coherence between motor cortex activity and electromyography (EMG) from hand muscles, highlighting synchronized oscillatory coupling between cortical and spinal motor systems (4, 5, 22). These foundational studies established a framework for subsequent investigations of EMG–EMG and corticomuscular coherence, which the present work extends to forearm extensor regions using high-density surface EMG decomposition. Beta oscillations have been shown to transmit linearly from the motor cortex to tonically active muscles (23). Both descending corticospinal pathways and ascending sensory inputs contribute to CMC, with coherence strength modulated by movement and muscle activity (24). High-density electromyography (HDsEMG) enables detection of beta bursts in individual motor units (MUs), providing a direct measure of corticospinal beta transmission (25). This offers a novel opportunity to bridge the gap in our understanding of how beta bursts propagate through the corticospinal tract and influence MU activity. In addition, investigating beta bursts across multiple force levels may provide novel insights into how MUs synchronize with beta oscillations and how corticospinal transmission adapts to changes in force output, potentially informing models of motor impairment in PD.

To date, only two studies have tracked the propagation of beta bursts from the cortex to the MUs, both focusing on the tibialis anterior in the lower limb (25, 26). Other studies that tracked beta propagation have relied on bipolar EMG recordings to examine CMC (27, 28), but these lack the spatial resolution to isolate individual MU activity. The extent to which beta bursts exhibit similar transmission dynamics in the upper limb remains unclear, especially given the distinct corticospinal organization of upper limb muscles (29).

In this study, we investigate the cortical-peripheral relationship of beta bursts using EEG and HDsEMG during isometric forearm contractions. Specifically, we aim to *1*) assess the reliability of HDsEMG in detecting beta bursting in the upper limb, *2*) determine whether peripherally recorded MU activity reflects cortical beta bursts, and *3*) examine how beta bursts differ between the brain and muscle across different force levels. To our knowledge, this is the first upper-limb study to combine transient beta-burst analysis, MU-level CMC via HDsEMG decomposition, and EEG-MU burst coherence. We hypothesize that beta bursts in forearm muscles will not exhibit distinct characteristics depending on contraction intensity, given prior evidence that corticomuscular coherence across force levels stayed unchanged (26). In addition, we expect that cortical beta bursts will be time-locked with MU activity in the forearm extensors, supporting direct corticospinal transmission. By addressing these questions, this study seeks to advance understanding of the role of beta bursts in motor control and their potential implications for neurorehabilitation and closed-loop DBS strategies in PD.

MATERIALS AND METHODS

Participants

We recruited 24 participants (26.0 ± 3.3 yr, 6 females) who were all right-handed as self-reported. None of the participants had a reported history of neurological conditions or upper limb injuries. All participants gave written informed consent before participation in the study. The study was approved by the Imperial College Research Ethics Committee (ICREC number 6715837) and conducted in accordance with the Declaration of Helsinki.

Experimental Design

At the start of the experiment, participants performed a single maximum voluntary wrist extension for 5 s to estimate the level of maximum voluntary contraction (MVC). To achieve an accurate maximum force level, verbal encouragement was provided. The MVC was calculated as the 95% percentile of the peak force value to reduce the influence of transient spikes from noise or vibration, providing a stable and reproducible estimate consistent with plateau-based approaches used in previous studies (30, 31). This value was then used as a reference for the rest of the experiment to adjust the torque of the isometric contraction ramps to the participants' individual strength levels.

Participants then familiarized themselves with the force trajectory task through practice trials at 10%, 20%, and 30% MVC, where force trajectories and a trapezoidal force template were displayed on a monitor. Contractions were limited to low force levels (10–30% MVC) to minimize fatigue during 60-s tasks and to ensure reliable HDsEMG decomposition, which becomes less accurate at higher forces due to MUAP overlap and cancellation (32, 33). Each trial consisted of 3 s rest (baseline), a linear increase in force to the target contraction level for 4s (ramp up), 60 s steady contraction at the target MVC level (plateau), 4 s linear decrease in force to rest (ramp down), and 3 s rest (baseline). The main experiment started after 3 min of rest and consisted of three blocks (1 at each MVC level: 10%, 20%, and 30% MVC) with five trials per block. The order of MVC blocks was randomized, and there was a 60-s rest between 10% and 20% MVC trials and a 120-s rest between 30% MVC trials to minimize muscle fatigue effects.

Data Acquisition

Force recordings.

The HRX-1 interface robot (34) was used to record torque during isometric wrist extension. This device was table-mounted, and the participants' dominant forearms were strapped to the device, with the back of the hand resting against the robot handle. Participants were seated at a height allowing the elbow joint angle to be set at 90° of flexion. The force signal was sampled at 24 Hz and recorded through custom MATLAB scripts. The force and trapezoidal ramp visuals were displayed using the Psychophysics Toolbox Version 3 (35–37) written in MATLAB R2023a (38).

HDsEMG recordings.

HDsEMG was acquired from the extensor carpi ulnaris (ECU) and extensor carpi radialis (ECR) muscle regions of the dominant forearm via a configuration of four 64-electrode grids [5 columns × 13 rows; gold-coated; 1-mm diameter; 4-mm interelectrode distance (IED); OT Biolettronica]. Multiple grids were used in the configuration to maximize the total MUs identified from the HDsEMG recordings by using a large number of electrodes and short IED (39). The grids were arranged to form a 256-electrode array (see Fig. 1*A*), with grids centered around the muscle belly while in parallel with the direction of muscle fibers. Grid placement was guided by anatomical landmarks (e.g., lateral epicondyle, ulnar styloid) and palpation of the target region during isometric contraction to locate the approximate muscle belly (see Fig. 1*C*). Although this procedure increases placement accuracy, we recognize that forearm extensor muscles are small, closely packed, and subject to interindividual variability, making definitive isolation difficult without imaging confirmation. To reflect this, each grid is referred to according to its approximate anatomical region as "ECU-proximal grid," "ECU-distal grid," "ECR-proximal grid," and "ECR-distal grid," indicating typical positioning over the extensor carpi ulnaris or extensor carpi radialis muscle bellies without implying exclusive sampling from a single muscle. To improve signal quality, the skin was shaved, gently abraded using abrasive paste, and cleansed using a 70% ethyl alcohol solution. To maintain electrode-to-skin contact, a perforated biadhesive foam infused with conductive paste was used. The grids were fastened in place with tape and elastic bands. A wet band was positioned around the wrist of the same arm and used as a reference to record the HDsEMG signals in monopolar mode. The HDsEMG signals were amplified (×150) using a multichannel EMG amplifier (Quattrocento, OT Bioelettronica, Turin, Italy), sampled at 2,048 Hz by a 16-bit A/D converter, and bandpass filtered from 10 to 500 Hz. Signals were recorded with the OTBioLab software (40).

EEG recordings.

The EEG data were recorded synchronously with HDsEMG recordings, with 19 dry electrodes using the DSI-24 (41). The electrodes were arranged according to the International 10-

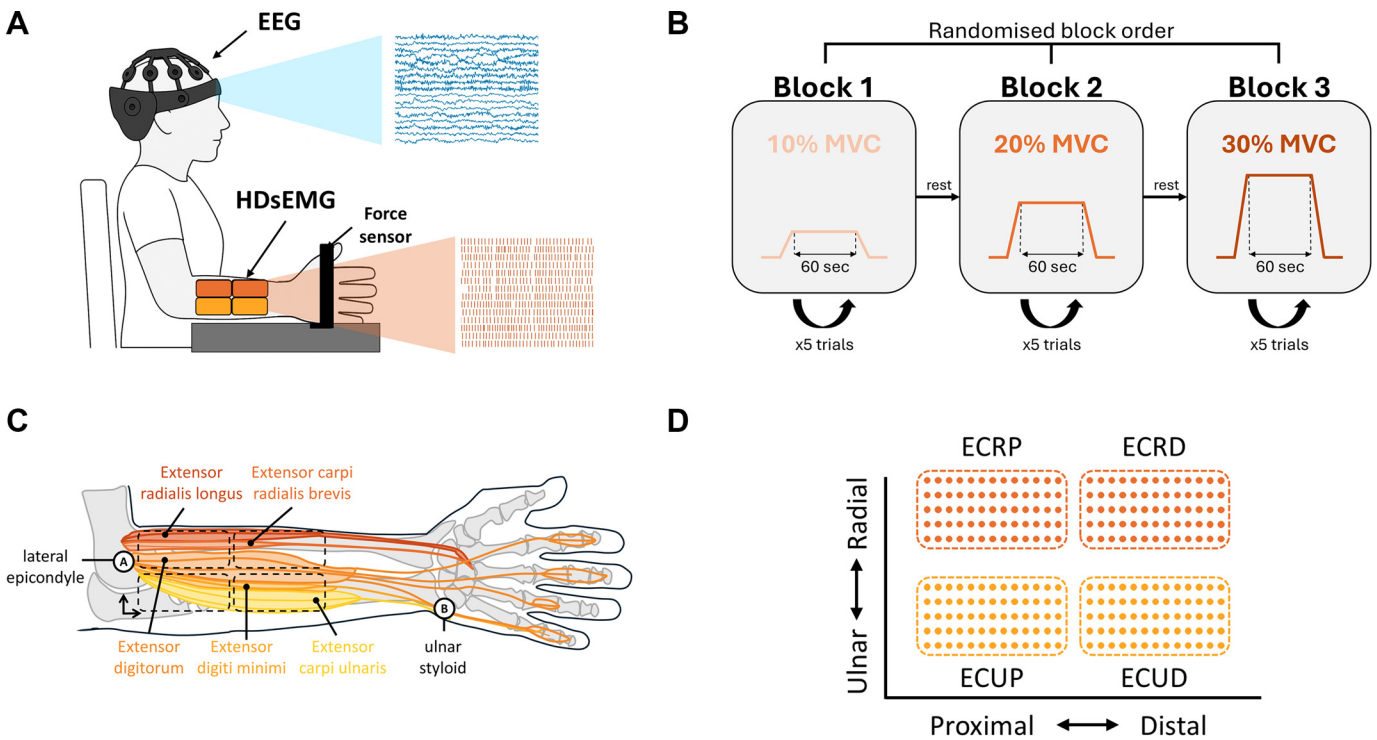

Figure 1. Overview of experimental setup and task paradigm. *A*: schematic of the EEG, HDsEMG, and torque recording setup during isometric wrist extension. *B*: participants performed a ramp-and-hold wrist extension task at 10%, 20%, and 30% maximum voluntary contraction (MVC) levels, following a randomized block design with rests in between trials and blocks. *C*: anatomical illustration of the right forearm showing approximate locations of the extensor muscle regions relative to the lateral epicondyle and ulnar styloid. HDsEMG grids were positioned over these regions using anatomical landmarks and palpation during isometric contraction. *D*: schematic of the four HDsEMG grids arranged in proximal-distal and ulnar-radial orientation. Grids are referred to as ECU-proximal (ECUP), ECU-distal (ECUD), ECR-proximal (ECRP), and ECR-distal (ECRD) to indicate their approximate anatomical placement without implying exclusive sampling from a single muscle.

20 system, Pz was used as the reference, Fpz as the ground, and signals were sampled at 300 Hz.

EEG, HDsEMG, and force signals were synchronized using a hardware trigger connected between systems to ensure precise temporal alignment.

Data Analysis

All offline analyses were conducted in MATLAB R2023a (38).

Decomposing HDsEMG into motor unit spike trains.

The recorded HDsEMG monopolar signals were decomposed into underlying MU activity using a previously validated blind-source separation algorithm (42, 43), with each grid being decomposed separately in accordance with previous work, which demonstrated that individual grid decomposition increased both the accuracy and yield of MU identification (44). This decomposition algorithm's accuracy has been demonstrated for isometric force contractions across a variety of muscles and force levels (45–47). Duplicate MUs within and between grids were identified and removed. MUs with more than 30% of the same discharge times were defined as duplicates. The decomposed discharge times of the MUs were manually inspected and edited in accordance with Ref. 48 to improve the decomposition accuracy using the MUedit software (49). The MU silhouette values (SIL) were calculated as a qualitative measure of evaluation of the decomposition accuracy. MUs with a SIL value of less than 0.9, firing delay of more than 5 s, or active window less than 50 s (of the 60-s plateau period) were discarded. Trials containing fewer than five distinct MUs were excluded to ensure reliable estimation of beta-band coherence, as previous experimental and computational work has shown that CST coherence estimates in the beta range are highly sensitive to the number of contributing MUs, with too few resulting in reduced spectral resolution and inflated variance (50, 51).

The amplification of common input in the CST depends on both the number of recruited MUs and their discharge rates, so to control for these factors, we normalized CSTs by matching the total number of firings across contraction levels within each participant. Although this procedure reduced the number of available trials, it ensured that included CSTs had sufficient resolution and stability for reliable estimation of beta-band coherence and bursting. For transparency, the full participant and MU counts are reported with detailed breakdowns in Supplemental Tables S1 and S2. The normalization step was done before CST construction by randomly selecting a subset of MUs for each trial, so that the total number of firings matched the minimum available across that participant's trial, allowing for a 10% tolerance range. This ensured that each CST contained the same number of firings, preventing trials with more MUs or higher firing rates from biasing coherence estimates. Figure 2 provides a detailed illustration of this process. After MU subsets were determined, new CSTs were reconstructed and coherence measures calculated. CSTs were obtained by summing binary MUs for the 60-s plateau period only. The CST average discharge rates were calculated by averaging the instantaneous discharge rates. For corticomuscular coherence (CMC) and bursting analysis, the MUs were downsampled to 300 Hz before calculating the CST.

EEG preprocessing.

For the EEG preprocessing, the EEGLAB toolbox for MATLAB was used (52). The EEG signals were re-referenced to the linked ears, high-pass filtered at 1Hz, and then low-pass filtered at 45 Hz using a linear (zero-phase) noncausal FIR filter. This was done instead of bandpassing to avoid the problem of steeper than necessary low-pass slopes. Bad channels were removed automatically by removing flat channels (if flat for more than 5 s), channels with a substantial amount of noise (maximum acceptable high-frequency noise standard deviation of 4), and channels poorly correlated with other channels (minimum acceptable correlation with nearby channels of 0.8). Artifact subspace reconstruction was performed to correct small segments of bad data with a standard deviation cutoff for the burst removal of 6 and using a Euclidean distance. This was followed by performing independent component analysis (ICA) for artifact rejection. Components were flagged and removed if they had a more than 70% probability of being a muscle, eye, or heart artifact. A current source density transform, more commonly known as a surface Laplacian, was applied to the EEG data using the CSD toolbox (53, 54) as recommended by Ref. 55. EEG analysis was conducted on the C3 channel only due to its location over the sensorimotor cortex contralateral to the forearm according to the 10-20 system.

Coherence analysis.

An essential aspect of our study involved examining the relationship between continuous EEG signals and spiking MU activity, as well as investigating intramuscular coherence (IMC) of MUs from different extensor muscle regions. The Neurospec 2.11 toolbox (David; 56, 57) for MATLAB (38), which was previously validated (23, 58, 59), was integrated to calculate the coupling strength and frequency content between time series and point process data, or between two spike trains.

The IMC was estimated for trials with at least two MUs by splitting the MU pool into two randomly chosen groups of equal size and calculating their coherence using Neurospec's two-channel spectral analysis. The IMC was the average of coherence estimates over 100 iterations. The CMC was estimated between the downsampled to 300 Hz CST, and EEG C3 channel using Neurospec's two-channel spectral analysis. Both the IMC and CMC were estimated for MUs from individual grids, pairs of grids, and all four grids together.

All coherence analysis was conducted with segments of 2 s and multitapers (three tapers). Significant coherences were identified using the upper 95% confidence limit estimates from Neurospec (60). These are calculated using the formula $1-0.05^{[1/(L-1)]}$, where L represents the number of segments used in computing the Fourier transform.

Beta burst extraction.

The beta bursting activity from the EEG was extracted based on previously developed methods, which first calculate the signal's amplitude within a specific frequency range and then identify instances where amplitude fluctuations surpass a predefined threshold (8, 11, 61). Burst analysis was only conducted on CSTs from joint MUs of the two grids over the ECU muscle and for trials with at least five MUs.

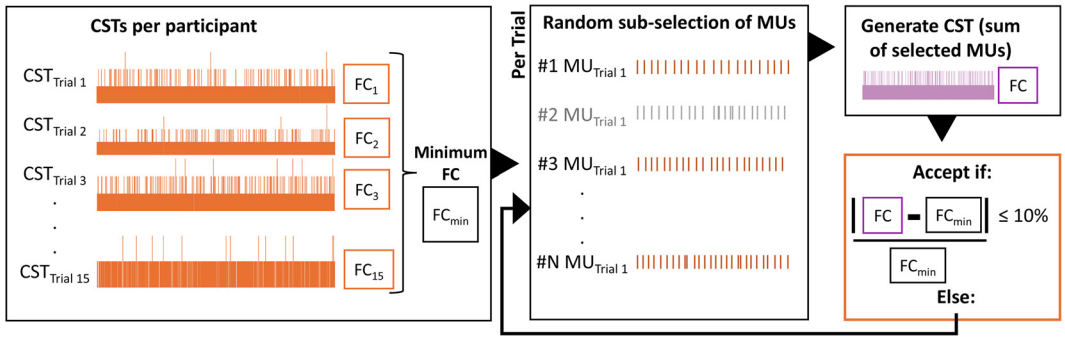

Figure 2. Resampling procedure for cumulative spike train (CST) generation. Schematic of the resampling approach used to equalize the number of motor unit (MU) firings across trials within each participant. *Left*: for each participant, firing counts (FCs) were calculated from the identified MUs in each trial, and the minimum firing count (FC_{min}) across all trials was determined. *Middle*: for each trial, a random subset of MUs was selected. *Right*: a CST was then generated by summing the selected MU spike trains. Trials were accepted if their firing count was within 10% of FC_{min}; otherwise, resampling was repeated. This procedure ensured that CSTs across trials contained an equal number of firings, preventing differences in MU yield or firing rate from biasing coherence estimates.

Participant-specific bursting thresholds were determined by bandpass filtering each trial between 13 and 30 Hz ("bandpass" function in MATLAB, zero-phase FIR), taking the upper envelope of the signal (using spline interpolation over local maxima separated by at least 30 samples), and then normalizing the signal. The 75th percentile threshold was then calculated for the envelope of each trial within a participant and averaged to determine the threshold used for that participant. After determining the burst threshold, bursts were defined as periods of longer than 100 ms of the signal envelope crossing the threshold, to ensure bursts included at least one full oscillation cycle in the beta range. The procedure is illustrated in Fig. 3.

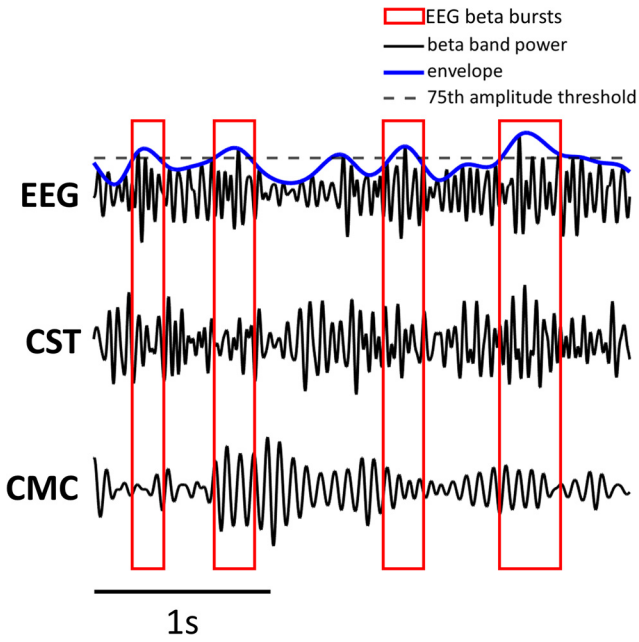

Figure 3. Burst detection and segmentation procedure. Electroencephalography (EEG) signals were filtered in the beta band (13–30 Hz), the envelope was extracted, and bursts were defined as periods where the envelope exceeded the 75th percentile threshold (dashed line) and were at least 100 ms long. Detected burst "ON" and "OFF" segments were aligned across EEG, cumulative spike trains (CST), and corticomuscular coherence (CMC) based on locations of EEG beta bursts.

Time-frequency analysis.

The time-frequency analysis of the CST and EEG was performed using the continuous wavelet transform, implemented through MATLAB's *cwt* function (38) between 1 and 45 Hz. CMC was computed using magnitude-squared wavelet coherence via the *wcoherence* function in MATLAB. A comparable method was applied to track the temporal progression of IMC, using a custom MATLAB script based on the *wcoherence* function. Similar to the coherence analysis, to assess IMC, the MU pool was divided into two randomly selected subpools of equal size. Magnitude-squared wavelet coherence was then computed between the CSTs of these MU subpools. This process was repeated 100 times, with each iteration using a different MU subpool configuration. The final IMC value was derived by averaging the coherence estimates obtained across all iterations.

Before identifying ON and OFF events, EEG, CST, and CMC wavelets were z-scored per frequency bins, and torque was upsampled to 300 Hz. ON and OFF events were identified in the EEG, CST, and CMC wavelets based on the locations of beta bursts identified in the EEG signals. Events of ON bursting were defined as 500 ms windows around bursts whose midpoint occurred at least 250 ms from the beginning or end of the 60-s plateau period. ON events were identified for each trial of a participant and then averaged within a trial. To prevent overlap between ON and OFF events, OFF events were defined as the periods between ON events, beginning 250 ms after the previous ON event and ending 250 ms before the next ON event, that were longer than 500 ms. Windows of overlap 50 ms and step size 500 ms were averaged across the OFF periods. ON and OFF events were averaged across trials of participants, and percental mismatch was calculated for each participant. The percental mismatch across participants was then averaged. The percental mismatch between ON and OFF events was defined as (ON − OFF)/OFF × 100 and was also calculated for the torque to ensure bursting effects did not result from unstable force production.

Statistical Analysis

The statistical analysis was conducted using custom MATLAB scripts and the Neurospec 2.11 toolbox (for significant

coherences in the IMC and CMC as aforementioned). Results are reported as median and interquartile range (IQR) unless otherwise stated. To analyze significant beta activity differences between ON and OFF events in the time-frequency domain, we applied cluster-based permutation testing based on the approach of Ref. 62. This method addresses the multiple comparisons problem inherent in multidimensional data (time and frequency) by evaluating clusters of neighboring samples under a single permutation distribution, rather than assessing each sample independently. We performed 10,000 permutations with a univariate clustering threshold of 0.05, allowing for statistically robust identification of significant clusters in the beta range. This was not evaluated on the ON and OFF event difference for the EEG data, as the EEG data itself was used to define and identify the ON and OFF events. After testing for normality using the Shapiro–Wilk test, nonparametric Friedman tests were applied to look at differences in MU count between muscle groups and MVCs. Post hoc Dunn–Sidak tests were used for multiple comparisons of significant results.

RESULTS

MU Extraction Across Muscle Locations and Force Production

The distribution of MUs across grids (ECR and ECU grids) and force levels (10%, 20%, and 30% MVC) before thresholding for ≥5 MUs can be observed in Fig. 4 across 24 participants. The median number of MUs identified per trial for both muscles at 10%, 20%, and 30% MVC, respectively, were 2 (1-4), 1 (0-3), and 1 (0-2) for the ECR grid, and 4 (2-8), 3 (1-7), and 2 (0-9), for the ECU grid. A significant between-group difference was observed between the ECU and ECR grids

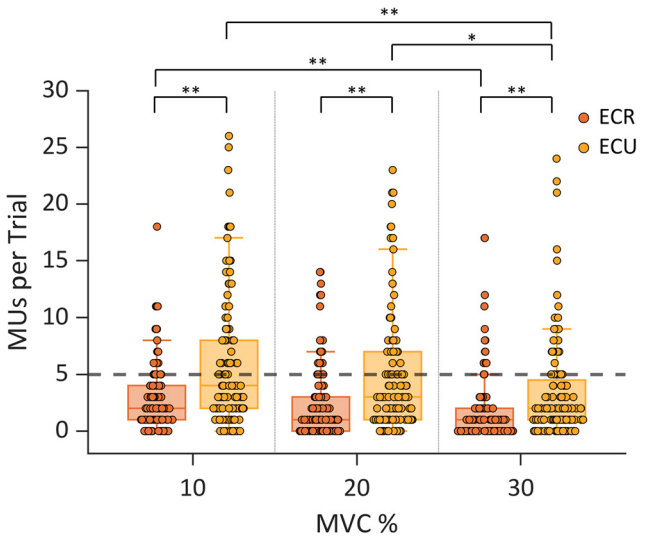

Figure 4. Number of motor units (MUs) per trial identified in extensor muscles for various grid combinations [ECR: extensor carpi radialis proximal (ECRP) + extensor carpi radialis distal (ECRD); ECU: extensor carpi ulnaris proximal (ECUP) + extensor carpi ulnaris distal (ECUD)] and target forces (10%, 20%, and 30% maximum voluntary contraction (MVC)). Each scatter marker represents the number of MUs per trial per participant (total trials per muscle = 360, participants = 24). Dashed horizontal line represents minimum threshold for MU filtering. *$0.01 < P < 0.05$; **$0.001 < P < 0.01$.

across all force levels (Friedman test: $P_{10\%} < 0.01$, $P_{20\%} < 0.01$, $P_{30\%} < 0.01$), indicating significantly more MUs in the ECU grid across all force levels. MU counts in the ECU grid decreased with increasing MVC, with significantly fewer MUs in 30% MVC versus 10% MVC (Friedman test: $P < 0.01$) and versus 20% MVC (Friedman test: $P < 0.05$). ECR grids MU counts also differed significantly between 10% MVC and 30% MVC (Friedman test: $P < 0.01$).

Across all trials with at least one successfully decomposed MU, the median number of MUs per trial per grid across all participants was 2 (1-4). MUs were initially identified from four electrode grids, ECRD, ECRP, ECUD, and ECUP, placed over the distal and proximal regions of the two muscles. However, due to low MU yield per individual grid (with only 12.14%, 16.34%, 22.13%, and 30.92% of trials exceeding the ≥5 MU threshold for ECRD, ECRP, ECUD, and ECUP grids, respectively), data from grids over the same muscle were combined to increase sampling density. This merging yielded a substantially higher proportion of usable trials: 26.69% of ECR grid trials and 42.21% of ECU grid trials exceeded the 5 MU threshold after grid-level merging.

Trials with a minimum number of MUs (≥5 MUs) and resampled CSTs across MVCs were included in the coherence analysis, with trial count, participants, and MU count across grid configurations seen in Supplemental Table S1. The MUs extracted demonstrated a decreasing number of MUs with target force, which aligns with previous findings (45).

Intramuscular Coherence

IMC across different grid combinations was investigated for the shared neural drive of the extensor muscles, which act synergistically during wrist extensions (Fig. 5). This analysis aimed to examine the functional coordination both within and between these muscles, as IMC indicates whether muscles work together as part of a functionally related group or a neural synergy (63). Understanding these coherence patterns can help identify which extensor muscle regions exhibit enhanced beta band frequencies. Although all force levels and grid combinations showed significant alpha (8–13 Hz) coherence, stronger and significant coherences in the beta band were observed consistently across MVCs only in the grids placed over the distal and proximal regions of the ECU (ECUD and ECUP), as well as in the shared coherence between these two grids. This suggests that specific MUs, where beta rhythms are more dominant or synchronized, are primarily located in the ulnar extensor region. These findings provide insight into where and how beta activity manifests in upper limb muscle activity. The limit for defining significant coherences was 0.034, corresponding to the 95% confidence limit determined by the number of segments in the Neurospec analysis. Furthermore, the ECU grid beta common neural drive increased with force, with a nonsignificant peak of 0.033 at 22.5Hz at 10% MVC, a significant peak of 0.037 at 21Hz at 20% MVC, and a significant peak of 0.048 at 24.5Hz at 30% MVC. These findings show that, similar to Ref. 64, muscles of the same synergistic group do not necessarily share the same neural drive, as the grids covering the radial and ulnar extensor regions share minimal common drive in this case. Despite increasing the number of MUs in the calculations when merging ECR and ECU grids, the IMC

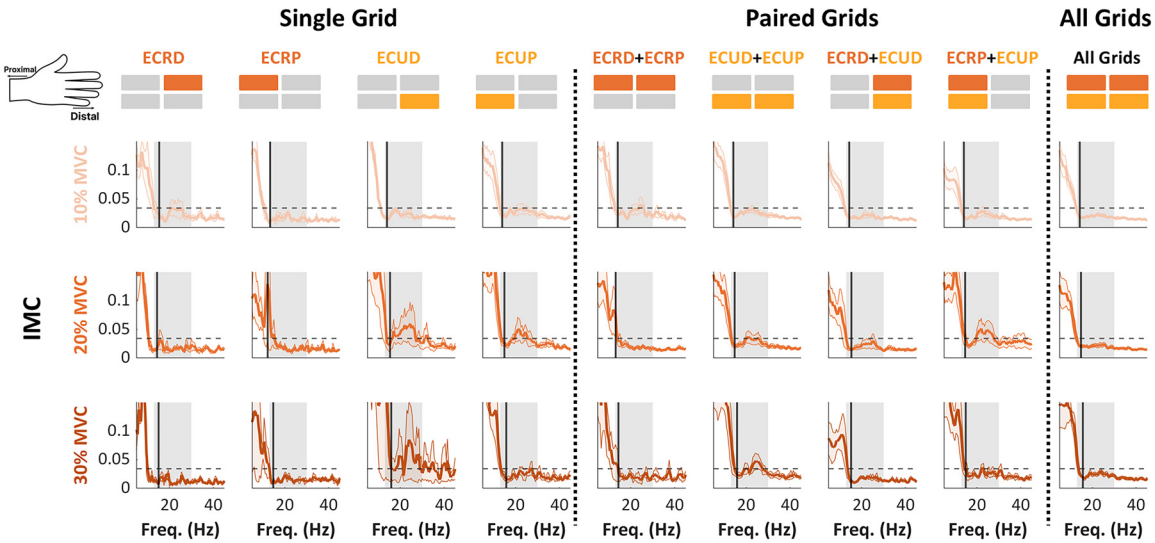

Figure 5. Intramuscular coherences across extensor muscle regions and force levels (10%, 20%, and 30% MVC). Horizontal dashed line is 95% significant threshold. Vertical solid line is mean discharge rate. Shaded area is standard error of mean. All Grids = ECRD + ECRP + ECUD + ECUP. ECRD, extensor carpi radialis distal grid; ECRP, extensor carpi radialis proximal grid; ECUD, extensor carpi ulnaris distal grid; ECUP, extensor carpi ulnaris proximal grid.

did not increase, further emphasizing this lack of shared neural drive.

Corticomuscular Coherence

The corticomuscular coherence (CMC) between cortical (EEG electrode C3 signals) and muscle (common input to decomposed ECU MUs quantified by the CST) was estimated across the three force levels (10%, 20%, and 30% MVC). The coherence spectra can be seen in Fig. 6. At 10% MVC, coherence remained relatively low across all frequencies, with no strong beta-band peak observed. At 20% MVC, coherence was slightly higher but still exhibited significant beta-band activity in the ECUD grid (0.032 at 21.09Hz). At 30% MVC, coherence increased, particularly in the beta range, where a significant peak was present at 25.2Hz (coherence 0.05), and 22.27Hz (coherence 0.048) in the ECRD and ECUD grids, respectively. These results show that beta band coherence becomes more pronounced with increasing force production in the distal forearm.

For completeness, we also ran IMC and CMC analyses, including all decomposed MUs without the ≥5 MU threshold. These results, provided in Supplemental Fig. S1 and S2, show qualitatively similar patterns but with reduced beta-band specificity and greater variability, particularly in the CMC estimates. This further supports the necessity of applying the filtering step for robust coherence analysis. To address coherence between synergist muscles, we also computed CST–CST coherence between ECU and ECR grid

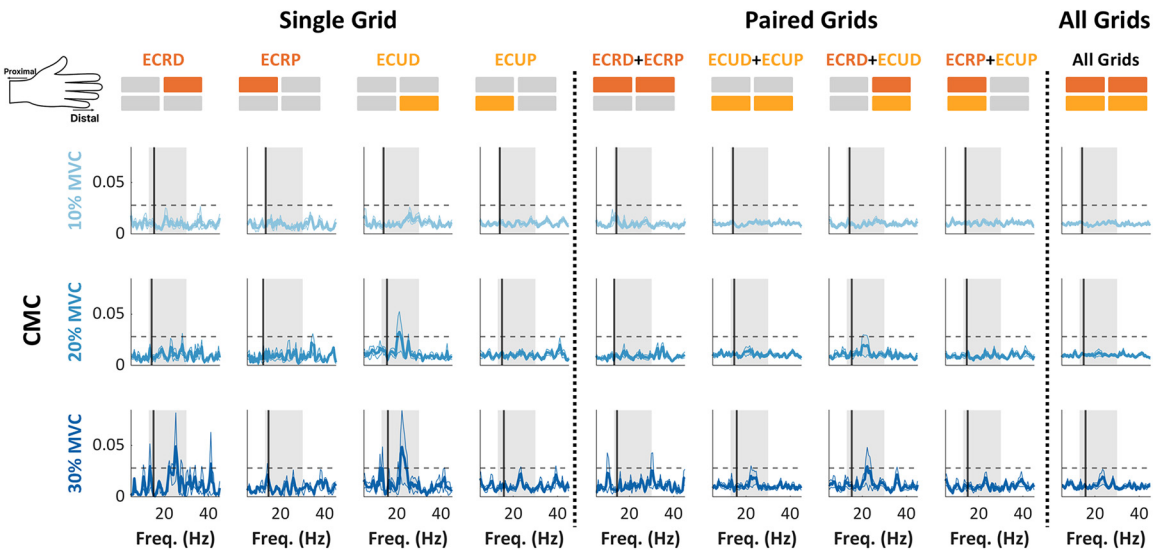

Figure 6. Corticomuscular coherence – average CMC (solid line) between ECU grid CST and EEG C3 averaged across trials and participants. Standard error mean (SEM) indicated by shaded area; 95% confidence limit (dashed line) and mean discharge rate (vertical solid line). All Grids = ECRD + ECRP + ECUD + ECUP. ECRD, extensor carpi radialis distal grid; ECRP, extensor carpi radialis proximal grid; ECUD, extensor carpi ulnaris distal grid; ECUP, extensor carpi ulnaris proximal grid.

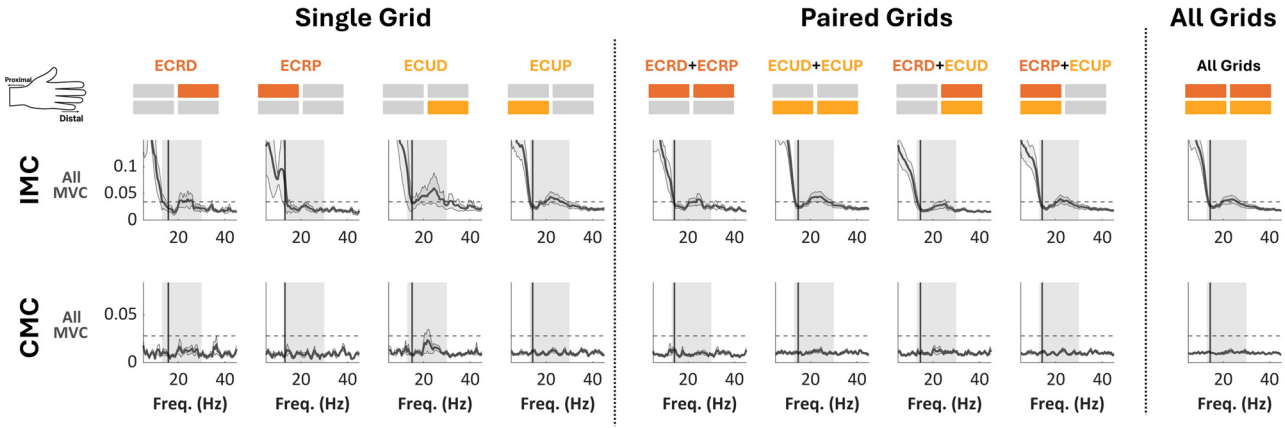

Figure 7. Intramuscular and corticomuscular coherence across extensor muscles at all force levels together (10%, 20%, and 30% MVC). CSTs have not been resampled for consistent firings. All Grids = ECRD + ECRP + ECUD + ECUP. ECRD, extensor carpi radialis distal grid; ECRP, extensor carpi radialis proximal grid; ECUD, extensor carpi ulnaris distal grid; ECUP, extensor carpi ulnaris proximal grid.

regions. These results, provided in Supplemental Fig. S3, showed beta-band coherence, albeit with greater variability compared with within-muscle coherence.

Figure 7 presents data combined across all MVC levels and highlights the rationale for selecting the ECU grids as the primary focus for burst analysis. Among all electrode configurations, only the ECU grids demonstrated a consistent and statistically significant IMC beta-band peak, alongside the highest number of contributing participants ($n = 20$). In contrast, CMC beta activity was only observed in the ECUD grid and did not reach statistical significance. The raw (unresampled) MU counts, trials, and participants contributing to Fig. 7 are detailed in Supplemental Table S2.

Focusing specifically on the ECU grids, 130 trials from 20 participants—representing 36.1% of all trials and 83.3% of participants—were included in the burst analysis, combining trials across all force levels (10%, 20%, and 30% MVC) from the joint ECU grids. This selection was based on the observation that grids covering the ECU yielded a greater number of identified MUs and a stronger common beta drive compared with those covering the ECR region.

Beta activity, though transient, is evident across brain, muscles, and their connectivity during sustained extensor contraction. In Fig. 8, periods in the CST, CMC, and torque have been identified based on the "ON" and "OFF" periods of the EEG beta bursts. When averaging across trials, beta ON events appear brief and clearly distinguishable from OFF periods, not only in the EEG but also in the CST and CMC. This emphasizes the transient nature of beta bursts beyond the cortex. Cluster-based permutation analyses confirmed significant transient differences between ON and OFF periods in both muscle beta power within the CST and brain-muscle connectivity in the CMC. Importantly, no significant modulation in grip force was observed during beta ON

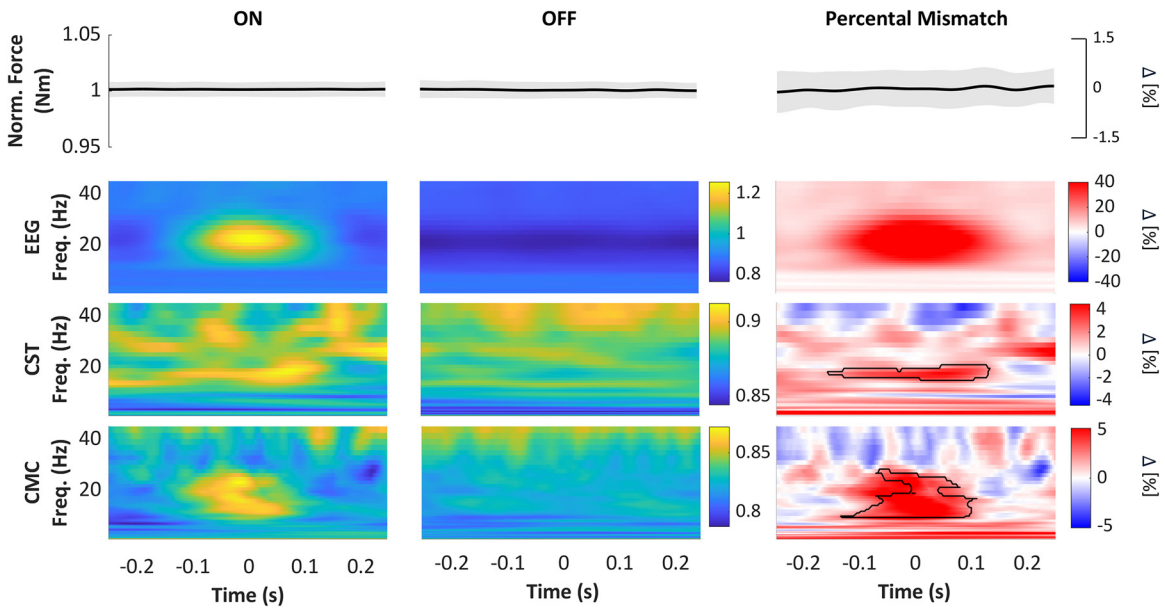

Figure 8. Neural and peripheral bursting activity at burst occurrences in the EEG. Burst ON and OFF events were averaged across trials. From *top* to *bottom*: normalized force, wavelet transformed EEG, CST, and CMC with t = 0 representing the center of ON periods (*left*), OFF periods (*middle*), and percental mismatch between ON and OFF periods (*right*). Black outlines represent the most significant clusters in the beta band ($P < 0.05$).

events, with force fluctuations remaining within 1% between ON and OFF periods, indicating that the observed beta bursts were not driven by changes in motor output. These bursts were synchronized across cortical and peripheral sites, with CST beta activity occurring simultaneously to EEG bursts.

DISCUSSION

We investigated the cortical-peripheral relationship of beta activity and bursts between the output of spinal motor neurons and brain oscillations during isometric forearm contractions, providing new evidence of synchronized beta-burst activity across the motor cortex and forearm muscle regions in the upper limb. We assessed the reliability of HDsEMG for detecting beta bursts across various force levels and extensor muscle regions and examined the alignment of beta bursts at the cortical and peripheral levels. Our findings reveal that beta activity in MU pools of the upper limb occurs in discrete, transient bursts that strongly reflect and overlap with cortical beta bursts, extending previous observations made in the lower limb (25). We also show that the ECU grids exhibit stronger shared beta neural input than the ECR grids, highlighting muscle-specific differences in common beta input. Similar to previous corticomuscular beta-burst research (25, 27, 28), CST beta bursts occurred simultaneously with EEG beta bursts. These findings provide new insights into corticospinal dynamics during voluntary muscle contractions by being the first to examine beta-burst synchronization between the cortex and MUs in the upper limb, and by exploring how these bursts vary across different force levels.

Regional Differences in Shared Neural Drive within the Forearm Extensors

Our results suggest regional differences in shared neural drive across the forearm extensors, as evidenced by significantly high beta synchronization across all MVCs in the ECU grids, but not ECR grids. These differences should not be interpreted as reflecting single-muscle isolation, but rather as evidence of distinct coupling patterns across forearm muscle regions. This indicates that the distribution of common beta input is not uniform across forearm extensors and may reflect muscle-specific modulation of synaptic drive within the beta range. Although we cannot determine from these data whether the sources of input differ qualitatively between muscles, the disparity in synchronization strength may relate to differences in functional roles and control strategy. While the ECU primarily stabilizes the wrist and facilitates both wrist extension and ulnar deviation (movement of the wrist toward the little finger) (65), the ECR provides a balancing force during wrist extension, counteracting excessive ulnar deviation, and contributing to overall wrist extension (66). Given their biomechanical distinctions, the two muscles may activate independently based on specific movement demands, potentially requiring greater synchronization among MUs in the ECU to support its stabilizing role. Although functionally related muscles often exhibit a stronger shared drive (67, 68), our findings imply that this relationship may vary according to each muscle's biomechanical function. Finally, exploratory analyses did not reveal consistent intermuscle beta-burst synchrony between ECU and ECR, suggesting that coordinated beta transmission across these synergists may be weak or variable during low-force isometric tasks.

The presence of alpha band (8–12 Hz) IMC across all muscles may reflect synchronized oscillations associated with motor control and stability, as previously observed in both upper and lower limb tasks (69–71). This low-frequency coupling may relate to the minimum discharge rate required for MU recruitment and could serve to enhance postural stability or regulate movement execution, particularly during slower, controlled contractions (72, 73). However, in this study, we assumed that activity from the ECR and ECU could be distinguished in HDsEMG recordings, despite potential signal contamination from coactivation of surrounding extensor muscles, such as the extensor digitorum, and interindividual variations in muscle anatomy relative to grid placements. Although minor differences were observed between distal and proximal grids, they were grouped together due to the limited number of decomposed MUs. As expected from previous studies on the upper limb (74, 75), we observed a low number of decomposed MUs from the extensors, likely due to the fusiform architecture of the ECU and ECR. Compared with pennate muscles, such as the tibialis anterior, fusiform muscles have parallel muscle fibers and exhibit less variety in MU action potential shapes toward the skin surface, which may reduce the effectiveness of decomposition techniques (76).

Corticomuscular Beta Transmission and Relationship to Force

We observed a trend toward increasing beta CMC with higher force levels; however, statistical significance was not fully achieved, likely due to interindividual variability (77, 78). This trend aligns with the notion that stronger corticospinal coupling may support forceful contractions, as previously shown in muscles such as the first dorsal interosseous, tibialis anterior, and knee flexors/extensors at low-to-moderate forces (79–81). However, findings across the literature remain mixed, with some reporting a decreasing MU synchronization strength at higher forces (82) and others showing no clear trend (83), likely due to a limitation of MU discrimination at lower contraction intensities. Although we did not explicitly test directionality using directed or partial coherence, previous studies have demonstrated that beta-band corticomuscular coherence predominantly reflects descending drive from motor cortex to spinal (4, 23, 24). Our findings are therefore interpreted within this established framework.

Our findings are further contextualized by recent evidence from Ref. 26, which showed that cortical beta band oscillations are uniformly projected to the entire motor neuron pool across a full range of recruitment thresholds in the tibialis anterior. In their study, CMC remained stable across contraction intensities, and conduction delay estimates confirmed consistent corticospinal transmission via fast-conducting fibers, regardless of MU size. Although our results show a nonsignificant trend toward increased beta CMC with force, the lower overall coherence values and interindividual variability observed in our upper-limb dataset may reflect anatomical or functional differences from the lower limb. Unlike the tibialis anterior, a unipennate muscle with a relatively homogeneous MU pool, the extensors are smaller, fusiform muscles that

may receive more distributed or muscle-specific descending inputs. Taken together, these findings suggest that while the core transmission mechanism for beta input may be conserved across muscles, its observable strength and variability could be influenced by muscle architecture and task demands.

Reliability of HDsEMG in Detecting Beta Bursts in the Upper Limb

Our findings confirm that HDsEMG reliably detects transient beta bursts in forearm extensor muscles, reinforcing its utility for studying upper limb corticospinal dynamics. We found that peripheral beta bursts were not only transient but synchronized with cortical bursts, with CST beta activity being time-locked to EEG bursts, similar to findings of Refs. 25 and 27. Prior work shows that CSTs improve signal-to-noise ratio and spectral resolution by emphasizing shared synaptic input across MUs (50, 51). This contrasts with approaches using single MUs (84) and was particularly advantageous for our analysis of transient beta bursts. As no significant changes in produced torque were observed and torque differences between burst ON and OFF periods were minimal ($\leq$1.5%), reinforcing that beta bursts are unlikely to directly modulate force production. Instead, they may contribute indirectly to sustaining motor output or monitoring sensorimotor states. Yet, Zicher et al. (85) found that when beta activity was modeled as transient bursts rather than continuous oscillations, these bursts reached levels capable of inducing small fluctuations in force. Similarly, Echeverria-Altuna et al. (27) demonstrated that brain-muscle neural synchronization occurs in brief, frequency-specific bursts, even during sustained motor tasks, further supported by our results. Beta bursts may play an indirect role in sustaining motor activity, potentially by monitoring peripheral states (24, 86) or through alternative neural pathways not examined in this study, such as intracortical connectivity or nonlinear cortical-peripheral integration of sensory information. However, further research is required to confirm these hypotheses.

Limitations

Despite the strengths of this study, several methodological limitations should be considered when interpreting the findings. First, given the target muscle size and limitations inherent with noninvasive methods, such as HDsEMG, the ability to detect deep MUs accurately in the forearm muscles or a high number of decomposed MUs was hindered. Although we positioned grids using palpation and anatomical landmarks, the small size and close proximity of forearm extensors mean that some signal contamination from adjacent muscles cannot be excluded. Second, trials with low MU counts were discarded, which could introduce sampling bias and affect the generalizability of the findings. In particular, although we recorded from 24 participants and identified over 2,000 MUs across all trials, the requirement of $\geq$5 MUs per trial and the CST normalization procedure reduced the number of trials included in coherence and burst analyses. Although this inevitably decreased the sample size for some conditions, it was essential to ensure reliable beta-band estimates. Third, as only low-force contractions ($\leq$30% MVC) were assessed, results may not fully generalize to higher-force tasks where decomposition reliability decreases. Lastly, the variability in force maximum and muscle size across participants further complicates the interpretation, as strength and beta power were seemingly correlated.

Conclusion

Future research should investigate how corticomuscular beta bursting behaves across a range of task conditions, including dynamic movements and prolonged exertion, to better understand how these bursts contribute to motor control during more natural, functional tasks and provide further ecological validity to the observed beta-burst dynamics. Extending these findings to clinical populations, such as individuals with Parkinson's disease, stroke, or those using prosthetic devices, could yield crucial information on how altered corticospinal coupling impacts motor behavior in these populations. To ensure broader generalizability, future studies should examine other muscles and incorporate intracortical recordings or high-density EEG to refine coherence analysis.

In conclusion, this study provides novel insights into how beta bursts contribute to corticospinal interactions during motor control, specifically in the upper limb muscles and across force levels. Our findings advance our understanding of the neural drive and motor stability in reflecting cortical beta activity, as well as understanding the time-locking of cortical and peripheral bursts. These insights could have important implications for neurorehabilitation strategies, particularly for individuals with motor impairments, such as Parkinson's disease, where beta bursts are a well-established neural biomarker of its motor symptoms, particularly rigidity and bradykinesia. Moreover, the ability to reliably detect peripheral beta bursting may inform the development of closed-loop DBS systems by providing an accessible biomarker for adaptive neuromodulation. Tracking beta dynamics at the MU level could allow more precise, feedback-driven stimulation paradigms targeting abnormal beta synchronization in Parkinson's disease. By validating the ability to track beta bursts across the corticospinal tract in upper limb muscles, similar to the tibialis anterior, using HDsEMG as a robust neural signal, we pave the way for future innovations in neuroengineering, particularly for investigating changes in the brain during neuromodulation interventions.

DATA AVAILABILITY

Source data for this study are not publicly available due to privacy and ethical restrictions. The source data are available to verified researchers upon request by contacting the corresponding author.

SUPPLEMENTAL MATERIAL

Supplemental Figs. S1–S3 Supplemental Tables S1 and S2: https://figshare.com/s/9c0cf48e78b741dab2dc.

ACKNOWLEDGMENTS

Preprint is available at https://doi.org/10.1101/2025.05.22.655541.

GRANTS

C.G. is supported by the UKRI Centre for Doctoral Training in AI for Healthcare, UK Research and Innovation (EP/S023283/1);

A.P.V. is supported by Marie Skłodowska-Curie grant agreement and European Union's Horizon Europe research and innovation programme (101151398). S.H. is supported by the Edmond and Lily Safra Fellowship. C.G., R.V., and S.H. are supported by the UK Dementia Research Institute, Care Research & Technology Centre.

DISCLOSURES

No conflicts of interest, financial or otherwise, are declared by the authors.

AUTHOR CONTRIBUTIONS

C.G., A.P.V., D.F., and S.H. conceived and designed research; C.G. performed experiments; C.G., A.P.V., and S.H. analyzed data; C.G., A.P.V., D.F., and S.H. interpreted results of experiments; C.G. prepared figures; C.G. drafted manuscript; C.G., A.P.V., D.F., R.V., Y.F.T., and S.H. edited and revised manuscript; C.G., A.P.V., D.F., R.V., Y.F.T., and S.H. approved final version of manuscript.

REFERENCES

1. **Engel AK**, **Fries P.** Beta-band oscillations — signalling the status quo? *Curr Opin Neurobiol*, 20: 156–165, 2010. doi:10.1016/J.CONB.2010.02.015.
2. **Kilavik BE**, **Zaepffel M**, **Brovelli A**, **MacKay WA**, **Riehle A.** The ups and downs of beta oscillations in sensorimotor cortex. *Exp Neurol* 245: 15–26, 2013. doi:10.1016/J.EXPNEUROL.2012.09.014.
3. **Feingold J**, **Gibson DJ**, **Depasquale B**, **Graybiel AM.** Bursts of beta oscillation differentiate postperformance activity in the striatum and motor cortex of monkeys performing movement tasks. *Proc Natl Acad Sci USA* 112: 13687–13692, 2015.
4. **Baker SN**, **Olivier E**, **Lemon RN.** Coherent oscillations in monkey motor cortex and hand muscle EMG show task-dependent modulation. *J Physiol* 501: 225–241, 1997. doi:10.1111/J.1469-7793.1997.225BO.X.
5. **Kilner JM**, **Baker SN**, **Salenius S**, **Jousmäki V**, **Hari R**, **Lemon RN.** Task-dependent modulation of 15-30 Hz coherence between rectified EMGs from human hand and forearm muscles. *J Physiol* 516: 559–570, 1999. doi:10.1111/J.1469-7793.1999.0559V.X.
6. **Baker AP**, **Brookes MJ**, **Rezek IA**, **Smith SM**, **Behrens T**, **Smith PJP**, **Woolrich M.** Fast transient networks in spontaneous human brain activity. *eLife* 3: e01867, 2014. doi:10.7554/eLife01867.
7. **West TO**, **Duchet B**, **Farmer SF**, **Friston KJ**, **Cagnan H.** When do bursts matter in the primary motor cortex? Investigating changes in the intermittencies of beta rhythms associated with movement states. *Prog Neurobiol* 221: 102397, 2023. doi:10.1016/j.pneurobio.2022.102397.
8. **Little S**, **Bonaiuto J**, **Barnes G**, **Bestmann S.** Human motor cortical beta bursts relate to movement planning and response errors. *PLoS Biol* 17: e3000479, 2019. doi:10.1371/JOURNAL.PBIO.3000479.
9. **Torrecillos F**, **Tinkhauser G**, **Fischer P**, **Green AL**, **Aziz TZ**, **Foltynie T**, **Limousin P**, **Zrinzo L**, **Ashkan K**, **Brown P**, **Tan H.** Modulation of beta bursts in the subthalamic nucleus predicts motor performance. *J Neurosci* 38: 8905–8917, 2018. doi:10.1523/JNEUROSCI.1314-18.2018.
10. **Tinkhauser G**, **Pogosyan A**, **Little S**, **Beudel M**, **Herz DM**, **Tan H**, **Brown P.** The modulatory effect of adaptive deep brain stimulation on beta bursts in Parkinson's disease. *Brain* 140: 1053–1067, 2017. doi:10.1093/BRAIN/AWX010.
11. **Tinkhauser G**, **Pogosyan A**, **Tan H**, **Herz DM**, **Kühn AA**, **Brown P.** Beta burst dynamics in Parkinson's disease OFF and ON dopaminergic medication. *Brain* 140: 2968–2981, 2017. doi:10.1093/BRAIN/AWX252.
12. **O'Keeffe AB**, **Malekmohammadi M**, **Sparks H**, **Pouratian N.** Synchrony drives motor cortex beta bursting, waveform dynamics, and phase-amplitude coupling in Parkinson's disease. *Journal of Neuroscience* 40: 5833–5846, 2020. doi:10.1523/JNEUROSCI.1996-19.2020.
13. **Pauls KAM**, **Korsun O**, **Nenonen J**, **Nurminen J**, **Liljeström M**, **Kujala J**, **Pekkonen E**, **Renvall H.** Cortical beta burst dynamics are altered in Parkinson's disease but normalized by deep brain stimulation. *Neuroimage* 257: 119308, 2022. doi:10.1016/j.neuroimage.2022.119308.
14. **Vinding MC**, **Tsitsi P**, **Waldthaler J**, **Oostenveld R**, **Ingvar M**, **Svenningsson P**, **Lundqvist D.** Reduction of spontaneous cortical beta bursts in Parkinson's disease is linked to symptom severity. *Brain Commun* 2: fcaa052, 2020. doi:10.1093/braincomms/fcaa052.
15. **Abbasi O**, **Hirschmann J**, **Storzer L**, **Özkurt TE**, **Elben S**, **Vesper J**, **Wojtecki L**, **Schmitz G**, **Schnitzler A**, **Butz M.** Unilateral deep brain stimulation suppresses alpha and beta oscillations in sensorimotor cortices. *Neuroimage* 174: 201–207, 2018. doi:10.1016/J.NEUROIMAGE.2018.03.026.
16. **Lofredi R**, **Tan H**, **Neumann WJ**, **Yeh CH**, **Schneider GH**, **Kühn AA**, **Brown P.** Beta bursts during continuous movements accompany the velocity decrement in Parkinson's disease patients. *Neurobiol Dis* 127: 462–471, 2019. doi:10.1016/J.NBD.2019.03.013.
17. **Luoma J**, **Pekkonen E**, **Airaksinen K**, **Helle L**, **Nurminen J**, **Taulu S**, **Mäkelä JP.** Spontaneous sensorimotor cortical activity is suppressed by deep brain stimulation in patients with advanced Parkinson's disease. *Neurosci Lett* 683: 48–53, 2018. doi:10.1016/J.NEULET.2018.06.041.
18. **Spooner RK**, **Hizli BJ**, **Bahners BH**, **Schnitzler A**, **Florin E.** Modulation of DBS-induced cortical responses and movement by the directionality and magnitude of current administered. *NPJ Parkinsons Dis* 10: 53–10, 2024. doi:10.1038/s41531-024-00663-9.
19. **Yao P**, **Sharma A**, **Abdi-Sargezeh B**, **Liu T**, **Tan H**, **Hahn A**, **Starr P**, **Little S**, **Oswal A.** Beta burst characteristics and coupling within the sensorimotor cortical-subthalamic nucleus circuit dynamically relate to bradykinesia in Parkinson's disease. *Mov Disord*. 40: 962–968, 2025. doi:10.1002/MDS.30163.
20. **Brovelli A**, **Ding M**, **Ledberg A**, **Chen Y**, **Nakamura R**, **Bressler SL.** Beta oscillations in a large-scale sensorimotor cortical network: directional influences revealed by Granger causality. *Proc Natl Acad Sci USA* 101: 9849–9854, 2004. doi:10.1073/PNAS.0308538101.
21. **Salenius S**, **Portin K**, **Kajola M**, **Salmelin R**, **Hari R.** Cortical control of human motoneuron firing during isometric contraction. *J Neurophysiol* 77: 3401–3405, 1997. doi:10.1152/JN.1997.77.6.3401.
22. **Conway BA**, **Halliday DM**, **Farmer SF**, **Shahani U**, **Maas P**, **Weir AI**, **Rosenberg JR.** Synchronization between motor cortex and spinal motoneuronal pool during the performance of a maintained motor task in man. *J Physiol* 489: 917–924, 1995. doi:10.1113/JPHYSIOL.1995.SP021104.
23. **Ibáñez J**, **Del Vecchio A**, **Rothwell JC**, **Baker SN**, **Farina D.** Only the fastest corticospinal fibers contribute to β corticomuscular coherence. *J Neurosci* 41: 4867–4879, 2021 [Erratum in *J Neurosci* 42: 5127–5128, 2022]. doi:10.1523/JNEUROSCI.2908-20.2021.
24. **Witham CL**, **Riddle CN**, **Baker MR**, **Baker SN.** Contributions of descending and ascending pathways to corticomuscular coherence in humans. *J Physiol* 589: 3789–3800, 2011. doi:10.1113/JPHYSIOL.2011.211045.
25. **Bräcklein M**, **Barsakcioglu DY**, **Del Vecchio A**, **Ibáñez J**, **Farina D.** Reading and modulating cortical β bursts from motor unit spiking activity. *J Neurosci* 42: 3611–3621, 2022. doi:10.1523/JNEUROSCI.1885-21.2022.
26. **Abbagnano E**, **Pascual-Valdunciel A**, **Zicher B**, **Ibáñez J**, **Farina D.** Projection of cortical beta band oscillations to a motor neuron pool across the full range of recruitment (Preprint). *BioRxiv*, 2025. doi:10.1101/2025.03.18.644010.
27. **Echeverria-Altuna I**, **Quinn AJ**, **Zokaei N**, **Woolrich MW**, **Nobre AC**, **van Ede F.** Transient beta activity and cortico-muscular connectivity during sustained motor behaviour. *Prog Neurobiol* 214: 102281, 2022. doi:10.1016/J.PNEUROBIO.2022.102281.
28. **Simpson TG**, **Godfrey W**, **Torrecillos F**, **He S**, **Herz DM**, **Oswal A**, **Muthuraman M**, **Pogosyan A**, **Tan H.** Cortical beta oscillations help synchronise muscles during static posture holding in healthy motor control. *Neuroimage* 298: 120774, 2024. doi:10.1016/J.NEUROIMAGE.2024.120774.
29. **Tinkhauser G**, **Shah AS**, **Fischer P**, **Peterman K**, **Debove I**, **Nygyuen K**, **Nowacki A**, **Torrecillos F**, **Khawaldeh S**, **Tan H**, **Pogosyan A**, **Schuepbach M**, **Pollo C**, **Brown P.** Electrophysiological differences between upper and lower limb movements in the human subthalamic nucleus. *Clin Neurophysiol* 130: 727–738, 2019. doi:10.1016/J.CLINPH.2019.02.011.
30. **Balshaw TG**, **Fry A**, **Maden-Wilkinson TM**, **Kong PW**, **Folland JP.** Reliability of quadriceps surface electromyography measurements

is improved by two vs. single site recordings. *Eur J Appl Physiol* 117: 1085–1094, 2017. doi:10.1007/S00421-017-3595-Z.

31. **Memarzadeh A**, **Morrison AP**, **Merzbach V**, **Ferrandino M**, **Arora A**, **Claydon-Mueller LS**, **Khanduja V.** Validating the cambridge protocol: reliability of hip muscle strength measurements using a motorized dynamometer and electromyography. *Sports Health* 14: 740–746, 2022. doi:10.1177/19417381211056869.
32. **Dick JMT**, **Tucker K**, **Hug F**, **Besomi M**, **van Dieën JH**, **Enoka RM**, **Besier T**, **Carson RG**, **Clancy EA**, **Disselhorst-Klug C**, **Falla D**, **Farina D**, **Gandevia S**, **Holobar A**, **Kiernan MC**, **Lowery M**, **McGill K**, **Merletti R**, **Perreault E**, . . . **Hodges PW.** Consensus for experimental design in electromyography (CEDE) project: application of EMG to estimate muscle force. *Journal of Electromyography and Kinesiology* 79: 102910, 2024. doi:10.1016/J.JELEKIN.2024.102910.
33. **Martinez-Valdes E**, **Laine CM**, **Falla D**, **Mayer F**, **Farina D.** High-density surface electromyography provides reliable estimates of motor unit behavior. *Clin Neurophysiol* 127: 2534–2541, 2016. doi:10.1016/J.CLINPH.2015.10.065.
34. ***HumanRobotix London.***: *robots for neuromechanics and research*. (n.d.). Retrieved February 24, 2025, from https://www.humanrobotix.co.uk/.
35. **Brainard DH.** The psychophysics toolbox. *Spat Vis* 10: 433–436, 1997. doi:10.1163/156856897X00357.
36. **Kleiner M**, **Brainard D**, **Pelli D**, **Ingling A**, **Murray R**, **Broussard C.** What's new in psychtoolbox-3. *Perception* 36: 1–16, 2007.
37. **Pelli DG.** The VideoToolbox software for visual psychophysics: transforming numbers into movies. *Spat Vis* 10: 437–442, 1997. doi:10.1163/156856897X00366.
38. **The MathWorks Inc.** *MATLAB version: 9.14.9 (R2023a)*. The MathWorks Inc. https://uk.mathworks.com/.
39. **Caillet AH**, **Avrillon S**, **Kundu A**, **Yu T**, **Phillips ATM**, **Modenese L**, **Farina D.** Larger and denser: an optimal design for surface grids of emg electrodes to identify greater and more representative samples of motor units. *eNeuro* 10: ENEURO.0064–ENEU23.2023, 2023. doi:10.1523/ENEURO.0064-23.2023.
40. **OT Bioelettronica.** (n.d.). *OTBiolab: A free software for signal analysis*. OT Bioelettronica. Retrieved February 24, 2025, from https://otbioelettronica.it/en/software/.
41. **DSI-24 - Wearable Sensing | Dry EEG.** (n.d.). Retrieved October 9, 2025, from https://wearablesensing.com/dsi-24/.
42. **Holobar A**, **Minetto MA**, **Farina D.** Accurate identification of motor unit discharge patterns from high-density surface EMG and validation with a novel signal-based performance metric. *J Neural Eng* 11: 016008, 2014. doi:10.1088/1741-2560/11/1/016008.
43. **Negro F**, **Muceli S**, **Castronovo AM**, **Holobar A**, **Farina D.** Multi-channel intramuscular and surface EMG decomposition by convolutive blind source separation. *J Neural Eng* 13: 026027, 2016. doi:10.1088/1741-2560/13/2/026027.
44. **Caillet AH**, **Phillips ATM**, **Farina D**, **Modenese L.** Motoneuron-driven computational muscle modelling with motor unit resolution and subject-specific musculoskeletal anatomy. *PLoS Comput Biol* 19: e1011606, 2023. doi:10.1371/JOURNAL.PCBI.1011606.
45. **Del Vecchio A**, **Casolo A**, **Negro F**, **Scorcelletti M**, **Bazzucchi I**, **Enoka R**, **Felici F**, **Farina D.** The increase in muscle force after 4 weeks of strength training is mediated by adaptations in motor unit recruitment and rate coding. *J Physiol* 597: 1873–1887, 2019. doi:10.1113/JP277250.
46. **Farina D**, **Holobar A.** Characterization of human motor units from surface EMG decomposition. *Proc IEEE* 104: 353–373, 2016. doi:10.1109/JPROC.2015.2498665.
47. **Holobar A**, **Farina D**, **Gazzoni M**, **Merletti R**, **Zazula D.** Estimating motor unit discharge patterns from high-density surface electromyogram. *Clin Neurophysiol* 120: 551–562, 2009. doi:10.1016/J.CLINPH.2008.10.160.
48. **Del Vecchio A**, **Holobar A**, **Falla D**, **Felici F**, **Enoka RM**, **Farina D.** Tutorial: analysis of motor unit discharge characteristics from high-density surface EMG signals. *J Electromyogr Kinesiol* 53: 102426, 2020. doi:10.1016/J.JELEKIN.2020.102426.
49. **Avrillon S**, **Hug F**, **Baker SN**, **Gibbs C**, **Farina D.** Tutorial on MUedit: An open-source software for identifying and analysing the discharge timing of motor units from electromyographic signals. *J Electromyogr Kinesiol* 77: 102886, 2024. doi:10.1016/J.JELEKIN.2024.102886.
50. **Farina D**, **Negro F**, **Dideriksen JL.** The effective neural drive to muscles is the common synaptic input to motor neurons. *J Physiol* 592: 3427–3441, 2014. doi:10.1113/JPHYSIOL.2014.273581.
51. **Negro F**, **Farina D.** Factors influencing the estimates of correlation between motor unit activities in humans. *PLoS One* 7: e44894, 2012. doi:10.1371/JOURNAL.PONE.0044894.
52. **Delorme A**, **Makeig S.** EEGLAB: an open source toolbox for analysis of single-trial EEG dynamics including independent component analysis. *J Neurosci Methods* 134: 9–21, 2004. doi:10.1016/j.jneumeth.2003.10.009.
53. **Kayser J**, **Tenke CE.** Principal components analysis of Laplacian waveforms as a generic method for identifying ERP generator patterns: I. Evaluation with auditory oddball tasks. *Clin Neurophysiol* 117: 348–368, 2006a. doi:10.1016/J.CLINPH.2005.08.034.
54. **Kayser J**, **Tenke CE.** Principal components analysis of Laplacian waveforms as a generic method for identifying ERP generator patterns: II. Adequacy of low-density estimates. *Clin Neurophysiol* 117: 369–380, 2006b. doi:10.1016/J.CLINPH.2005.08.033.
55. **Kayser J**, **Tenke CE.** On the benefits of using surface Laplacian (current source density) methodology in electrophysiology. *Int J Psychophysiol* 97: 171–173, 2015. doi:10.1016/J.IJPSYCHO.2015.06.001.
56. **Halliday DM.** NeuroSpec: MATLAB routines for Multivariate Fourier Analysis of Time Series and/or Point Process Data. 2016. https://github.com/dmhalliday/NeuroSpec.
57. **Halliday DM.** Nonparametric directionality measures for time series and point process data. *J Integr Neurosci* 14: 253–277, 2015. doi:10.1142/S0219635215300127.
58. **Beck MM**, **Spedden ME**, **Lundbye-Jensen J.** Reorganization of functional and directed corticomuscular connectivity during precision grip from childhood to adulthood. *Sci Rep* 11: 22870, 2021. doi:10.1038/S41598-021-01903-1.
59. **Spedden ME**, **Beck MM**, **West TO**, **Farmer SF**, **Nielsen JB**, **Lundbye-Jensen J.** Dynamics of cortical and corticomuscular connectivity during planning and execution of visually guided steps in humans. *Cerebral Cortex (New York, N.Y.: 1991)* 33: 258–277, 2022. doi:10.1093/CERCOR/BHAC066.
60. **Rosenberg JR**, **Amjad AM**, **Breeze P**, **Brillinger DR**, **Halliday DM.** The Fourier approach to the identification of functional coupling between neuronal spike trains. *Prog Biophys Mol Biol* 53: 1–31, 1989. doi:10.1016/0079-6107(89)90004-7.
61. **Shin H**, **Law R**, **Tsutsui S**, **Moore CI**, **Jones SR.** The rate of transient beta frequency events predicts behavior across tasks and species. *eLife*, 6: e29086, 2017. doi:10.7554/eLife29086.
62. **Maris E**, **Oostenveld R.** Nonparametric statistical testing of EEG- and MEG-data. *J Neurosci Methods* 164: 177–190, 2007. doi:10.1016/J.JNEUMETH.2007.03.024.
63. **Laine CM**, **Valero-Cuevas FJ.** Intermuscular coherence reflects functional coordination. *J Neurophysiol* 118: 1775–1783, 2017. doi:10.1152/JN.00204.2017.
64. **Hug F**, **Del Vecchio A**, **Avrillon S**, **Farina D**, **Tucker K.** Muscles from the same muscle group do not necessarily share common drive: evidence from the human triceps surae. *J Appl Physiol (1985)* 130: 342–354, 2021. doi:10.1152/japplphysiol.00635.2020.
65. **Finsen L**, **Søgaard K**, **Graven-Nielsen T**, **Christensen H.** Activity patterns of wrist extensor muscles during wrist extensions and deviations. *Muscle Nerve* 31: 242–251, 2005. doi:10.1002/MUS.20237.
66. **Sawyer E**, **Sajjad H**, **Tadi P.** *Anatomy, shoulder and upper limb, forearm extensor carpi ulnaris muscle*. StatPearls: 2023. https://www.ncbi.nlm.nih.gov/books/NBK539760/.
67. **Kerkman JN**, **Daffertshofer A**, **Gollo LL**, **Breakspear M**, **Boonstra TW.** Network structure of the human musculoskeletal system shapes neural interactions on multiple time scales. *Sci Adv* 4: eaat0497, 2018. doi:10.1126/sciadv.aat0497.
68. **Laine CM**, **Martinez-Valdes E**, **Falla D**, **Mayer F**, **Farina D.** Motor neuron pools of synergistic thigh muscles share most of their synaptic input. *J Neurosci*, 35: 12207–12216, 2015. doi:10.1523/JNEUROSCI.0240-15.2015.
69. **Boonstra TW**, **Daffertshofer A**, **van Ditshuizen JC**, **van den Heuvel MRC**, **Hofman C**, **Willigenburg NW**, **Beek PJ.** Fatigue-related changes in motor-unit synchronization of quadriceps muscles within and across legs. *J Electromyogr Kinesiol* 18: 717–731, 2008. doi:10.1016/J.JELEKIN.2007.03.005.

70. **Boonstra TW**, **Danna-Dos-Santos A**, **Xie HB**, **Roerdink M**, **Stins JF**, **Breakspear M.** Muscle networks: connectivity analysis of EMG activity during postural control. *Sci Rep* 5: 17830, 2015. doi:10.1038/srep17830.
71. **de Vries IEJ**, **Daffertshofer A**, **Stegeman DF**, **Boonstra TW.** Functional connectivity in the neuromuscular system underlying bimanual coordination. *J Neurophysiol* 116: 2576–2585, 2016. doi:10.1152/JN.00460.2016.
72. **Danna-Dos-Santos A**, **Boonstra TW**, **Degani AM**, **Cardoso VS**, **Magalhaes AT**, **Mochizuki L**, **Leonard CT.** Multi-muscle control during bipedal stance: an EMG-EMG analysis approach. *Exp Brain Res* 232: 75–87, 2014. doi:10.1007/S00221-013-3721-Z.
73. **Kouzaki M**, **Masani K.** Postural sway during quiet standing is related to physiological tremor and muscle volume in young and elderly adults. *Gait Posture* 35: 11–17, 2012. doi:10.1016/J.GAITPOST.2011.03.028.
74. **Rojas-Martínez M**, **Mañanas MA**, **Alonso JF.** High-density surface EMG maps from upper-arm and forearm muscles. *J Neuroeng Rehabil* 9: 85, 2012. doi:10.1186/1743-0003-9-85.
75. **Rojas-Martínez M**, **Serna LY**, **Jordanic M**, **Marateb HR**, **Merletti R**, **Mañanas MÁ.** High-density surface electromyography signals during isometric contractions of elbow muscles of healthy humans. *Sci Data* 7: 397, 2020. doi:10.1038/s41597-020-00717-6.
76. **Francic A**, **Holobar A.** On the reuse of motor unit filters in high density surface electromyograms recorded at different contraction levels. *IEEE Access* 9: 115227–115236, 2021. doi:10.1109/ACCESS.2021.3104762.
77. **Fisher KM**, **Zaaimi B**, **Williams TL**, **Baker SN**, **Baker MR.** Beta-band intermuscular coherence: a novel biomarker of upper motor neuron dysfunction in motor neuron disease. *Brain* 135: 2849–2864, 2012. doi:10.1093/BRAIN/AWS150.
78. **Ushiyama J**, **Suzuki T**, **Masakado Y**, **Hase K**, **Kimura A**, **Liu M**, **Ushiba J.** Between-subject variance in the magnitude of corticomuscular coherence during tonic isometric contraction of the tibialis anterior muscle in healthy young adults. *J Neurophysiol* 106: 1379–1388, 2011. doi:10.1152/JN.00193.2011.
79. **Dal Maso F**, **Longcamp M**, **Cremoux S**, **Amarantini D.** Effect of training status on beta-range corticomuscular coherence in agonist vs. antagonist muscles during isometric knee contractions. *Exp Brain Res* 235: 3023–3031, 2017. doi:10.1007/S00221-017-5035-Z/FIGURES/2.
80. **McManus L**, **Flood MW**, **Lowery MM.** Beta-band motor unit coherence and nonlinear surface EMG features of the first dorsal interosseous muscle vary with force. *J Neurophysiol* 122: 1147–1162, 2019. doi:10.1152/JN.00228.2019.
81. **Ushiyama J**, **Masakado Y**, **Fujiwara T**, **Tsuji T**, **Hase K**, **Kimura A**, **Liu M**, **Ushiba J.** Contraction level-related modulation of corticomuscular coherence differs between the tibialis anterior and soleus muscles in humans. *J Appl Physiol (1985)* 112: 1258–1267, 2012. doi:10.1152/JAPPLPHYSIOL.01291.2011.
82. **Kline JC**, **De Luca CJ.** Synchronization of motor unit firings: An epiphenomenon of firing rate characteristics not common inputs. *J Neurophysiol* 115: 178–192, 2016. doi:10.1152/JN.00452.2015.
83. **Christou EA**, **Rudroff T**, **Enoka JA**, **Meyer F**, **Enoka RM.** Discharge rate during low-force isometric contractions influences motor unit coherence below 15 Hz but not motor unit synchronization. *Exp Brain Res* 178: 285–295, 2007. doi:10.1007/S00221-006-0739-5/FIGURES/6.
84. **Zheng Y**, **Zheng B**, **Qiang W**, **Peng Y**, **Xu G**, **Wang G**, **Li L**, **Shin H.** Corticomuscular coherence existed at the single motor unit level. *Neuroimage* 305: 120999, 2025. doi:10.1016/J.NEUROIMAGE.2024.120999.
85. **Zicher B**, **Ibáñez J**, **Farina D.** Beta inputs to motor neurons do not directly contribute to volitional force modulation. *J Physiol* 601: 3173–3185, 2023. doi:10.1113/JP283398.
86. **Baker SN.** Oscillatory interactions between sensorimotor cortex and the periphery. *Curr Opin Neurobiol* 17: 649–655, 2007. doi:10.1016/J.CONB.2008.01.007.